THE MOLECULAR MEASURING MACHINE

J. Kramar, J. Jun, W. Penzes, F. Scire, C. Teague, J. Villarrubia, E. Amatucci, D. Gilsinn

Precision Engineering Division

National Institute of Standards and Technology

Gaithersburg, MD 20899   USA

ABSTRACT

To help meet the measurement needs of industries preparing to manufacture future generations of nanoelectronic devices and circuits, the National Institute of Standards and Technology (NIST) has designed and built an instrument—called the Molecular Measuring Machine (M^3)—with the goal of measuring with one nanometer combined standard uncertainty the positions of features located anywhere within a 50 mm by 50 mm area. Achieving this capability for M^3 has required the development and integration of many forefront technologies: atomic-resolution scanning probes, high-accuracy interferometry for displacement measurements, and precision nanomotion generation. These have been combined in a controlled environment featuring ultra-high vacuum, acoustic and seismic vibration isolation, and millidegree-stability temperature control. In one demonstration of its capabilities, using the scanning tunneling microscope probe, M^3 imaged an array of laser-focused, atomically deposited chromium lines over a 5 μm by 1 mm area. An analysis of the image data yielded an average line spacing of 212.69 nm with an estimated expanded uncertainty of 0.01 nm, coverage factor, k, of two. This is based on a point-to-point expanded uncertainty of 50 nm (k = 2) for a 1 mm length measurement. In another measurement, the scanning tunneling microscope probe was able to continuously track a holographically-produced grating surface for 10 mm, counting out 49,996 lines and measuring an average line spacing of 200.01 nm with an expanded uncertainty of 0.01 nm (k = 2). This grating is now being used as a reference standard in the production of a spectrometer for the space-borne Advanced X-ray Astrophysics Facility being built by the National Aeronautics and Space Administration. Currently M^3 is undergoing a series of modifications. The motion actuators and guides are being refined, additional environmental and position sensors are being added, and a new machine controller system is being developed. These improvements should enable the capability for point-to-point measurements approaching the original goal. In addition to its measurement functions, M^3 can also serve as a tool for
exploring methods of manufacturing mechanical and electrical structures in the nanometer-size range.

INTRODUCTION

As feature sizes continue to shrink and densities continue to increase in integrated circuit devices [1] and in data storage media, the need for precise and accurate metrology continues to increase. In order to meet this increasing demand, at the National Institute of Standards and Technology (NIST) we have designed and built an instrument for performing two-dimensional coordinate measurements called the Molecular Measuring Machine (M^3) [2]. The metrology goal of M^3 is to achieve one nanometer combined standard uncertainty for any point-to-point measurements within a 50 mm by 50 mm measurement range while accommodating height differences of as much as one millimeter. The objective is also to be able to resolve nanometer-scale features with the imaging probe.

In this paper, we will describe the machine design including the concepts and principles that we strove to apply. We will then describe specimen measurements that have been made using the fully assembled instrument. The biggest sources of measurement uncertainty have been identified and will be discussed. We will discuss design modifications that are currently underway to reduce these uncertainties. We will conclude with comments on potential means of interaction with nanotechnology industries to promote and support accurate metrology.

MOLECULAR MEASURING MACHINE DESIGN

The Molecular Measuring Machine uses a combination of technologies to achieve its measurement goals. Scanning probe microscopy (SPM) is used for imaging specimen features. To achieve the desired range and resolution, stacked coarse and fine motion stages are used to generate the motion of the SPM probe relative to the surface. The displacement of the probe relative to the specimen in the XY plane is measured by a Michelson interferometer system. The entire system is
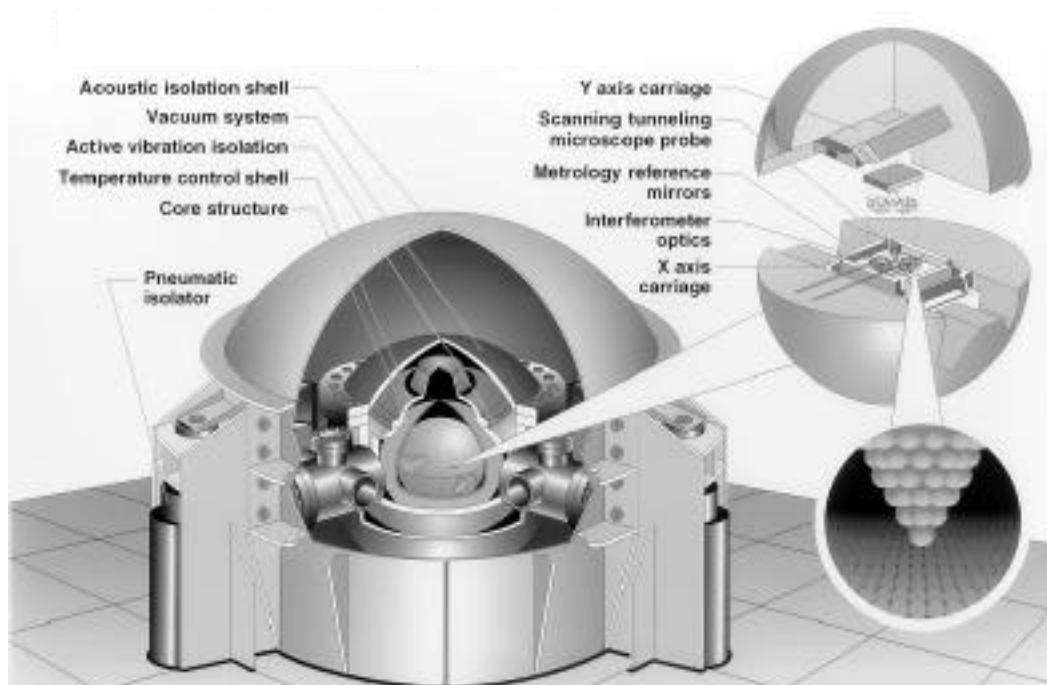
Figure 1. Cut away drawing of the Molecular Measuring Machine.

contained in a highly controlled environment. Careful temperature control and vibration control are needed. The system also operates in an ultra-high vacuum (UHV) chamber.

An overview cut-away drawing of M^3 is shown in Figure 1. The machine core is housed in a series of shells for controlling its environment. These are, in order, a temperature control shell, an in-vacuum, active vibration-isolation system, an ultra-high vacuum chamber, and an environmental chamber that can be sealed for acoustic isolation and that rests on pneumatic vibration-isolation legs. Cut into the machine core are the slideways for guiding the coarse-motion carriages. The coarse-motion carriages carry the fine motion stages. They in turn carry the specimen and the probe tip on the lower and upper carriage respectively. The specimen is located inside a mirrored box that provides the reference surfaces for the interferometric measurements. The rest of the interferometer optics are suspended from the upper carriage and move with the probe tip. The lasers that are used for the interferometers are located outside the environmental chamber. The light is brought in through viewports.

Machine Core and Motion Stages

The machine core is a copper sphere 350 mm in diameter. Oxygen-free high-conductivity (OFHC) copper is chosen for its machinability, dimensional stability, vacuum compatibility and thermal conductivity. The spherical shape is chosen to maximize the frequency of the natural resonance of the core. The core is manufactured in two pieces, the upper and lower

hemispheres. The coarse-motion slideways are rough cut into the hemispheres and finish machined by single-point diamond turning. A vee is used for the upper slideway and an inverted vee for the lower slideway. The slideways are oriented at 90° from each other to serve as X- and Y-axis motion guides. The slideways are electroless nickel plated to improve the hardness and the wear properties. Finally, they are lightly polished to remove any remaining high frequency variations. There are pockets machined into the core for holding the coarse-motion motors and the mechanisms for coupling the motion drives to the carriages.

The coarse-motion carriages are made of copper to match the core. The carriages have vee surfaces that conform to the slideways. The bearing surfaces are kinematically located Teflon [3] pads—three pads on one vee surface and two on the opposing surface. Teflon is chosen for its low friction properties and to minimize wear of the slideways. Some creep and wear of the Teflon is expected, but none has yet been detected.

An effort is made to decouple from the carriages any parasitic off-axis motion from the motors. For this purpose, secondary carriages, or trailers, are added between the motor drives and the main carriages. The trailers are made of copper and ride on Teflon pads on the diamond-machined slideways. Mechanically, the trailers surround the carriages without touching them. The motion is coupled from the trailers to the carriages by driving at each end through a free-floating ball between two anvils. Some backlash is built into the couplings

to avoid binding. The drive motion errors from the motors to the trailers are also decoupled by means of intervening bearings running on idler shafts and by coupling the motion through crossed cylinders.

The motors are located inside the core sphere. The requirements for the motors include: vacuum compatibility, 50 mm range with micrometer or better resolution, speed of at least 1 mm/s, compact size, minimum 25 N force generation, and minimal heat load. The original design called for piezoelectric linear stepper motors. Testing of early piezo motor designs showed that they were unable to generate sufficient force to drive the carriages. As a temporary solution, UHV-compatible electromagnetic rotary stepper motors with lead screws were used. All the measurements that have been done to date have used these motors. These motors meet all the design criteria except the requirement for minimal heat load. This has limited our ability to maintain constant temperature to the 5 mK fluctuation level.

A second stage of motion generation is built into each of the coarse-motion carriages. These are the fine-motion carriages. They are single-axis, flexure-guided stages that are aligned with the motion axis of their respective coarse-motion carriages. The motion actuators are piezoelectric stacks that generate a 10 μm range of motion. The motion resolution and noise is directly related to the resolution and noise of the controlling voltage. With proper care and filtering, sub-nanometer positioning is possible. Since the motion actuator is a piezoceramic element, some hysteresis and creep in the motion is unavoidable if simple voltage control is attempted. Instead, we use a closed-loop control system for positioning and scanning using the measurements from the interferometers as indicators of the position.

The design of the flexure motion guides is a compromise between mechanical stiffness and motion straightness. The flexure links need to be strong to achieve the former and weak for the latter. In the measurements performed to date, a design was used that weighted the compromise on the side of stiffness. Stiffness is necessary for maintaining stability of the probe-to-specimen spacing in the presence of vibrations, even given the low level of vibrations that pass through the vibration isolation systems. Higher stiffness also enables higher scan speeds. The compromise results in significant off-axis motion. The upper carriage is the worst with a coupling into the Z-axis of about 10%. Coupling into the horizontal axes also occurs, but it is compensated by the closed-loop position control. The angular motion errors are more significant in reaching the measurement uncertainty goal. The interferometers measure in a plane that is 10 mm above the sample level. Any tilt of the stages causes an Abbé error equal to the sine of the tilt angle times this height offset. The pitch and roll of the fine-motion carriages is

about 0.5 μrad per micrometer of motion, linear over the full 10 μm of travel to within a 0.2 μrad. This results in a net measurement error of about 5 nm for every micrometer of fine-motion carriage travel. Insomuch as this error is repeatable and measurable, it can be mapped and corrected.

Probe System

The probe that is being used for detecting and imaging features on the specimen is a scanning tunneling microscope (STM). The STM is chosen rather than the atomic force microscope (AFM) for the initial probe because it is simpler to design and build. It is also easier to achieve atomic resolution with the STM and on a greater number of specimens. Atomic-resolution imaging is an important goal for M^3 because we would like to validate the metrology system against known crystal geometries and spacings. It is planned to add an interchangeable AFM probe in the future so that electrically non-conductive specimens can also be measured.

The STM probe assembly is suspended from the upper fine-motion carriage. The STM is custom designed for M^3 because the limited space available does not allow the use of commercial UHV STM designs. For coarse positioning in the Z-axis, the STM uses a linear, piezoceramic, stepping motor. The motor consists of a piezoceramic assembly that moves inside a precision ground cylinder. The motor has a front and rear braking element and a central pusher. It works by sequentially braking the ends and pushing in an inchworm-like fashion. The motor has a 3 mm travel range and generates sub-micrometer steps. To date, the Z fine-motion actuator has been a piezoceramic tube scanner. The outer electrode of the tube is segmented so that by proper application of driving voltages, the tube can be bent to generate "superfine" X and Y axis motion [4]. Z-axis motion is generated by symmetrically driving all four quadrants. During measurement scans, the superfine X and Y scan capability is not used because the generated motion is not measured by the interferometers. The Z-axis fine-motion range is about 1.5 μm. Because of space constraints, the tube scanner had to be buried inside the coarse-motion piezo assembly. The entire assembly is less than 20 mm long and 30 mm in diameter.

The STM uses analog circuitry to control the probe specimen separation. The first-stage amplifier for measuring the tunneling current between the probe and the specimen is located inside the vacuum system on the fine-motion carriage. It has a fixed gain of 10^7 V/A. The external circuitry includes additional adjustable gain, a logarithmic amplifier to linearize the expected exponential nature of the tunneling signal, an adjustable control set point, a variable time-constant integrator to tune the response bandwidth, and high-voltage amplifiers to drive the piezoceramic actuators. The first mechanical resonance of the probe system that has significant phase lag is

at about 1 kHz. To avoid instability, the integrator time constant is adjusted so that the closed-loop gain at this frequency is kept below unity.

Metrology

The Molecular Measuring Machine is designed to be a two-dimensional measuring instrument. The primary metrology is performed by the X- and Y-axis Michelson interferometers. These measure the combined motion of the coarse and fine stages of the upper carriage relative to the combined stages of the lower carriage. The interferometers use an inside, dual-pass, differential optical configuration. This is a new variation of the outside differential configuration [5]. This results in an optical fringe spacing of one eighth of the red helium-neon laser wavelength. Fringe interpolation is done using heterodyne techniques.

The reference mirrors for the interferometry are carried on the lower fine-motion carriage. The mirrors are arranged in a box with the mirrored surfaces facing the inside. Angular tolerances are at the 10 µrad level and flatnesses are kept within 30 nm peak-to-valley. We call this precision optical assembly the metrology box. The box is made out of optically contacted Zerodur pieces. Test specimens are mounted on a removable sample holder that rests kinematically on the bottom of the metrology box.

The beamsplitter assemblies for the interferometer are suspended from the upper fine-motion carriage. Figure 2 is an exploded view of one of the beamsplitter assemblies, showing the arrangement of the optics and the path of the two interfering beams. The beamsplitter assemblies move with the base of the probe system and the specimen moves with the metrology box, as previously stated. In this way, the interferometers measure the displacement of the probe relative to the specimen. The unmeasured portions of the metrology
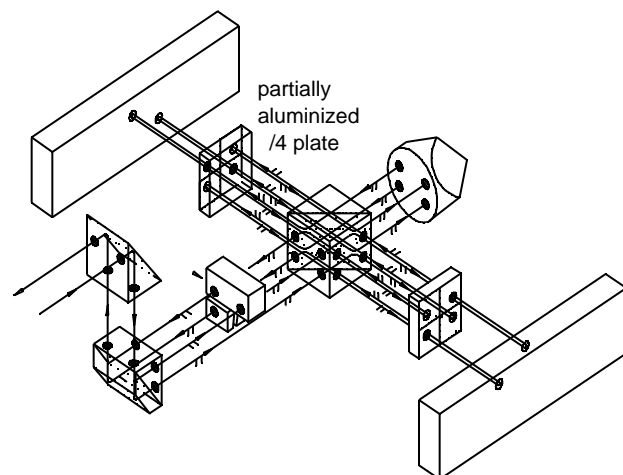
Figure 2. Exploded view of one of the interferometer beam-splitter assemblies showing the laser beam paths.

loop are from the metrology box mirrors to the specimen and from the beamsplitter assemblies through the common mounting plate and probe base to the STM probe tip. These unmeasured lengths are assumed constant during the course of a measurement. This assumption is checked by making repeatability measurements. At this stage in the development, 10 nm repeatability is typical.

We use a transverse-field, Zeeman-stabilized, red, helium-neon laser as our light source [6]. The heterodyne frequency of the orthogonally polarized output modes is about 450 kHz, phase-locked to an internal crystal-controlled frequency synthesizer. For fringe interpolation, we compare the zero-crossings of the AC-coupled reference and test beat-note signals with a time interval analyzer [7,8]. The time delay between the zero-crossings relative to the reference period is the fractional phase. The reference beat-note signal is from a sample of the laser output before it enters the vacuum system. The test signal is collected outside the vacuum system after the beams have propagated through the interferometer.

Environment Control

For the stability of the probe and specimen, for the stability of their relative spacing, and for repeatability and accurate metrology, it is necessary to implement thorough environmental control. This includes ambient composition control, temperature control, and isolation from vibrations coming from seismic and acoustic sources.

Ambient composition control is essential both from the point of view of the specimen stability and for the sake of accurate interferometry. As previously mentioned, it is one of our goals to measure the positions of atoms or molecules on crystal surfaces. Certainly, atomic resolution imaging with the STM has been demonstrated for many systems with in-air operation. However, there are many more crystal surfaces that are only stable against oxidation or hydrocarbon contamination in a highly controlled environment or in UHV. Similarly, less contamination of the probe tip is expected in vacuum, and better stability of the tunneling signal. With regard to accurate interferometry, ambient air interferometry is limited to a relative uncertainty of a few parts in 10^8 because of the difficulty in measuring and compensating for the changing refractive index of air with changing pressure, humidity, temperature and composition. Our metrology goal is for an interferometer accuracy an order of magnitude better than this. This is so that we can achieve a combined standard uncertainty from all sources of 2 parts in 10^8. For these reasons, we have enclosed the instrument in a UHV environment. Typical base pressure to date is 1×10^{-5} Pa. Maintaining UHV compatibility for all of the components has been one of the major challenges in the construction of M^3.

The low relative uncertainty of the metrology goal has also necessitated careful temperature control. Typical coefficients of thermal expansion (CTE) for structural materials are in the 10×10^{-6} °C ^{1} range. Better than millidegree control may therefore be necessary to keep this component of the uncertainty to a part in 10^9, depending on the specimen material. Even for a specimen like Zerodur with a CTE of 5×10^{-8} °C^{-1}, the thermal drift of the instrument itself will be an issue. To minimize the instrument component, the metrology box is made from Zerodur, as previously mentioned, and the mounting plate that couples the interferometer assembly to the probe system is made from Invar (CTE = 1.2×10^{-6} °C $^{-1}$). The temperature of the sample is measured with platinum resistance thermometers. The temperature of the instrument is also measured at several points. To control the temperature, the core is surrounded by a temperature control shell, a copper shroud that is wrapped with wires for resistive heating. The UHV chamber is kept a few degrees below the target temperature of 20 °C to act as a heat bath for cooling. The current through the wires is actively controlled to maintain the target temperature. Both the heater shell and the outer surface of the core are plated with matte-finish gold to maintain the stability of the radiative coupling between the two. The high thermal conductivity of the copper machine core promotes temperature uniformity, and the large thermal mass combined with relatively weak coupling to the outside environment promotes temperature stability. The time constant for the temperature control system when under vacuum is on the order of a day. In view of this, it is crucial to radically limit any heat sources inside the temperature control shell. In the measurements done to date, with infrequent operation of the electromagnetic coarse-motion motors, 5 mK temperature control was achieved. Without operating the motors, sub 1 mK temperature stability has been demonstrated.

The final element in the environmental control is the vibration isolation system. The machine structure and the motion carriages have been made as stiff as possible to limit the effects of vibrations on the probe-to-specimen spacing. Stiffness also enables higher scan speeds. Nevertheless, because of the limit to achievable stiffness inherent in a large translation range, thorough vibration isolation is necessary in order to achieve the stability required. Vibrations can be transmitted to the instrument both seismically through the support structure and acoustically through the air. Acoustic isolation is provided by housing the instrument in a UHV environment. An additional level of acoustic isolation is obtained by placing the UHV system on passive pneumatic mounts inside a hermetically sealed environmental control chamber. For seismic isolation, the environmental chamber itself is supported by pneumatic vibration isolation legs. Then yet another level of support-borne-vibration isolation is provided by a spring suspension system inside the UHV chamber. To date, this final vibration-isolation stage is passive with a natural resonance of about 4 Hz. Also, the motion of the suspended mass relative to its support is limited to the vertical degree of freedom by kinematic constraining rods. This is necessary to prevent angular motion of the internal interferometer components relative to the external laser sources. Active control of the kinematic rod lengths by means of piezoceramic actuators using control signals derived from accelerometers on the suspended mass has been contemplated, and will be implemented in the future if necessary. An active system would also help damp vibrations generated internally by the moving carriages.

Control, Data Acquisition and Display System

The overall control of the Molecular Measuring Machine and the data acquisition and real-time data display is done on a multi-processor computer with a real-time UNIX operating system [9]. Interface from the computer to the instrument is done through digital and analog input and output (I/O) cards on two busses—a proprietary I/O bus and an industry standard VME bus. All of the operating software beyond the common device drivers is custom written. The computer system has four processors. Of these, one is dedicated to reading the time interval data from the interferometer system and continuously calculating and updating the current position reading and storing it in a common data area. Another processor is dedicated to the control of the scanning systems and the acquisition and display of the data. The scanning and position control makes use of the interferometer-derived position data in the common data area. It uses this information to perform two-dimensional, closed-loop scan control. The acquired scan data at each pixel include readings from both interferometers and a digitized signal from the analog probe-control system that represents the probe height. Full 32 bit position data are required for the interferometer readings to maintain the desired resolution over the 50 mm range. The data are displayed on a computer monitor as they are acquired. This is necessary so that the operator can monitor the progress of the data acquisition, which may take as long as an hour per image. Operator interface to the software is through a command line interpreter. The interpreter has some logic and conditional-command capabilities. Because of this, it is straightforward to generate command files that can perform rather involved data acquisition. This allows extended, unattended operation once some preliminary understanding of the specific specimen characteristics has been gained.

MEASUREMENTS AND UNCERTAINTIES

The Molecular Measuring Machine has been used to measure several artifacts. The two that will be described here highlight the combined capability of long-range and high-accuracy measurements. These measurements will also serve as test cases from which estimates of the currently achievable measurement uncertainty can be determined.
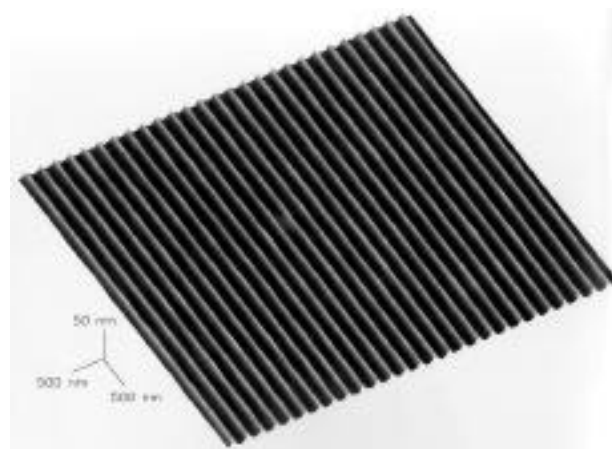
Laser-Focused-Atom-Deposition Chromium Grating

One type of specimen that has attracted our attention is the laser-focused-atom-deposition (LFAD) chromium grating. This is a line grating that is made by depositing neutral chromium atoms on a suitable substrate (in our case a silicon wafer) through a standing wave of high-intensity laser radiation, tuned near an atomic absorption line. The atoms interact with the radiation field and are focused into lines at the node spacing of the light. This technique for making chromium gratings was developed by McClelland, *et al.* [10] at NIST. The deposition takes place in a vacuum, so the node spacing is expected to be directly related to the laser frequency, which is accurately known. This specimen is then a good artifact for the validation of our metrology system. The calculated line spacing of the specimens we have examined is 212.78 nm with a preliminary expanded uncertainty of 0.02 nm, coverage factor, k, of 2 [11]. The pitch and the moderate 10 nm peak-to-valley line height on our specimen are in a convenient range for the STM probe. In the specimens we received, the grating lines are more than 100 μm long and the pattern extends for about 1 mm.

For measuring the average grating line spacing of this specimen, we acquired an image of a strip of the surface five micrometers wide and one millimeter long. The image was taken in segments spaced 5 μm apart, each segment 6 μm long and 5 μm wide. Each of these sub-image segments was acquired by scanning only the fine motion carriages. An example of a sub-image scan is shown in Figure 3. Between sub-images, the probe tip was retracted and the coarse motion carriage was advanced by 5 μm. Each sub-image overlaps its neighbors by 1 μm. Since the interferometer measures the combined displacement of the coarse and fine stages, the sub-images can be unambiguously combined into a single image. The overlapping regions serve as a verification only. Each sub-image cycle including the coarse-motion move took about an hour, for a total image time of about 8 days. After the total image was obtained, the beginning sub-image was scanned again to check for possible tip changes during the 8 day scan and to ensure repeatability. Several check images were also taken at various points along the millimeter image.

In order to extract an average pitch measurement from the data, two lines were selected, one near each end. The number of line spacings between the end lines was counted and the raw measurement of the distance between the two lines was determined from the interferometer coordinates. This raw distance measurement is corrected for two major effects, discussed below. The quotient of the corrected length measurement divided by the number of line spacings is the average pitch, with a standard uncertainty equal to the uncertainty in the length measurement divided by the number of line spacings. To verify the uniformity of the line spacing throughout the image, the line spacing in each sub-image was checked. We measured two different specimens of the LFAD chromium gratings. On one we measured an average pitch of 212.83 nm and on the other 212.69 nm. The expanded uncertainty for both measurements is 10 pm, k = 2.

The primary correction to the raw measurement is the correction for the alignment of the specimen with the interferometer axes of M^3. To measure this alignment, an additional series of images is taken in the orthogonal direction, along the grating lines. This gives a baseline over which to measure the alignment. With an adequate baseline, the alignment correction can be made as accurate as necessary.

An additional correction to the raw measurement is made to account for the cross coupling of the motion axes. The interferometer measures the position of the base of the probe system. All Z-axis motions are generated within the probe system. The tilt of the specimen with respect to the X and Y motion plane or any other height differences on the specimen result in varying Z axis positions at the measurement points. Any cross coupling of the Z-axis motion into the X- and Y-axes is therefore added to the probe position, but not measured by the interferometer. The amount of this cross coupling has

Figure 3. M^3 image of a 6 μm by 5 μm area of a laser-focused atomic-deposition Cr grating specimen.

been measured and a correction is applied to the length measurements based on this correction factor.

Holographic Gratings

Holographic gratings are another type of sample that we have measured. These gratings are made by the conventional photolithography technique of exposing a photoresist with a pattern and etching, except that in this case the pattern is generated not from a photomask, but by the holographic interference of two laser beams. With collimated or distant light sources, uniform gratings can be fabricated over large areas on the order of 100 mm by 100 mm. The particular samples we measured were made by the Center for Space Research at the Massachusetts Institute of Technology. The gratings we measured are used as reference artifacts in the production of holographic gratings for the x-ray spectrometer for the National Air and Space Administration's Advanced X-ray Astronomical Facility. We measured gratings of nominal 200 nm and 400 nm pitch.

For these measurements, a different algorithm for probing the specimens was used. Instead of acquiring a large image made up of many sub-images, a single, continuous line scan was made across the grating lines. To achieve the desired precision for the average pitch measurement, a 10 mm segment of the specimen was scanned. We aimed for a conservative average speed of 50 nm/s to minimize tip damage. The motion was generated by taking infrequent steps with the coarse motion motors. The compliance of the motor couplings and the effects of wind-up filtered the abruptness of the steps so that the maximum speed at the time of a step was only about 100 nm/s. This continuous line scan is used to count the number of lines over the measurement baseline. In order to check repeatability and to give a larger section of line over which to determine the end line positions, 5 μm by 5 μm images were taken at each end of the continuous line scan, centered on the starting and ending points. These images were repeated after the long line scan.

As in the LFAD chromium grating measurements, a series of images was taken along the grating lines to correct for the alignment of the grating with the metrology frame. The Z-axis cross-coupling correction factors were also applied. The resulting measurements for the grating line spacings are 400.80 nm with expanded uncertainty of 0.02 nm (k = 2), and 200.01 nm with expanded uncertainty of 0.01 nm (k = 2).

Uncertainty Estimates

The uncertainty for a given measurement depends on the details of the measurement. A description of the uncertainty calculations for one of the measurements of the LFAD chromium sample described above is presented as an illustrative example.

First, there are uncertainties associated with the interferometer displacement measurement itself. The wavelength of the helium-neon laser is the metric. The wavelength is the speed of light in the medium divided by the frequency. For M^3, the medium is a vacuum for which the speed of light is defined to be 299792458 m/s by international agreement. The frequency of the laser is determined by comparing with an iodine-stabilized He-Ne laser. Until now we have not been very rigorous with this comparison. The frequency is known to at least a part in 10^7, leading to a conservative standard uncertainty of 0.1 nm from this source for the 1 mm displacement measurement.

Another error in the interferometry results from what is commonly called polarization mixing. This is a periodic non-linearity caused by incomplete separation of the heterodyne modes by the interferometer beamsplitter. We have measured an error of 1 nm peak-to-peak at the fringe period of 80 nm for the M^3 interferometer system. This error adds to both ends of a given point-to-point measurement and could be correlated. Therefore, for the estimate of the uncertainty arising from this component, we take twice the peak error, or 1 nm.

The third error source in the interferometer system is the imperfect alignment of the measurement beams with the reference mirrors. Because of this misalignment, the optical path is longer than the intended measurement path by a factor equal to the cosine of the misalignment angle. For the measurement under consideration, no special care was taken in this alignment. As an upper bound to the potential error from this source, we use the maximum misalignment possible while still allowing interference of the two beams. This gives an angle, $_c$, of 6 mrad. The error is the cosine of the angle times the measurement length, 1 mm, which yields 20 nm. With conventional alignment techniques, it should be straightforward to measure the misalignment and therefore reduce it or correct for it to the 100 μrad level. This will yield a reduction of a factor of 4000 in the estimated uncertainty from this source. Note that the cosine error discussed here is distinct from the cosine error arising from the alignment of the interferometer with the motion axes. The latter is an error with which one must be concerned in one-dimensional metrology, but is directly measured in a three dimensional metrology system such as in M^3.

The errors discussed so far relate to the displacement measurement at the location of the interferometer laser beams. There remain errors in translating this measurement to the probe-sample interface, *i.e.*, in completing the metrology loop. One of the largest factors in this category for the M^3 metrology system is the Abbé offset error. Because of the inside interferometer configuration, it is impossible to bring the axis of the measurement beams down to the sample plane. The

Abbé offset for M^3 is about 10 mm. This offset multiplies by the sine of the angle of any pitch or roll of the carriages with respect to each other. For the coarse-motion carriage guides, to date we have been using a backup machine core with roughed out slideways instead of the precision slideways described above. For these ways, the carriage pitch and roll varies smoothly, roughly linearly, by about 25 µrad over the full 50 mm travel range. For a 1 mm translation, about 0.5 µrad is expected leading to an estimated error of 5 nm. In the measurement under consideration, only the X coarse motion carriage was moved, so there is no component from the Y coarse motion carriage. The fine-motion carriages also pitch and roll. These angular errors are also roughly linear in the stage position. The magnitude is about 0.5 µrad/µm travel. For the overall length measurement, we chose grating lines near the center of the fine motion scan range, within 1 µm. The error component for the Abbé error of the two fine motion carriages is therefore about 5 nm each. All three of these Abbé errors are uncorrelated. For a combined uncertainty estimate, we add them in quadrature yielding 9 nm.

Note that we ignore the yaw contribution to the Abbé error for the coarse and fine motion carriages. This is because the Abbé offset for this axis of angular motion is very small, on the order of one millimeter, because the two passes of the interferometer straddle the probe tip. The measured yaw error of the carriage motion is also small, about one tenth of the pitch and roll errors. Therefore this error component is about 100 times less than the pitch and roll Abbé error.

The other significant uncertainty component in closing the metrology loop is also due to a motion-generation error. This is the uncertainty in the Z-to-X and Z-to-Y coupling factor. The Z-to-X and Z-to-Y motion coupling is a result of using a piezoceramic directly (unguided) to generate the fine motion. For the measurement under consideration, only the coupling into the X-axis is relevant. This was measured to be 0.1 _X/_Z, and as previously stated, the measurements are corrected by multiplying the height difference by the coupling factor. But there is also a lack of repeatability of the coupling factor because of the hysteresis and creep of the piezoceramic. This leads to a relative standard uncertainty in the coupling factor of 0.02 _X/_Z. For this measurement, the height difference between the two end lines is 650 nm, so the standard uncertainty from this source is 13 nm.

Temperature variations and fluctuations affect both the instrument and the specimen. For the instrument, again the effect on the unmeasured portions of the metrology loop is the key issue. The path from the reference mirrors to the sample holder is Zerodur, so temperature effects of that piece are be negligible. The sample holder is copper with a CTE of 2×10^{-5} °C^{-1}. The active length is about 25 mm. The relevant material from the interferometer optics to the probe tip is stainless steel with a similar active length and a CTE of 1×10^{-5} °C^{-1}. The important temperature factor is not the absolute temperature, but the variation in the temperature during the coarse of the measurement. This was about 5 millidegrees Celsius, resulting in correlated uncertainty components of 3 nm and 1 nm, respectively. For the sample, the relevant temperature factor is the uncertainty in the absolute temperature at the time of the measurement. This is also about 5 millidegrees Celsius. This temperature uncertainty is multiplied by the measurement length, 1 mm, and the CTE of the silicon substrate of the specimen, 2×10^{-6} °C^{-1}. The resulting estimated uncertainty for this component is only 10 pm.

There is also an uncertainty component associated with the alignment of the specimen within the metrology frame. As for the Z-to-X coupling, a correction is made to the overall measurement based on the alignment, but the uncertainty in the determination of the alignment leads to a component in the overall uncertainty estimate. The estimated alignment uncertainty is 100 µrad. The cosine of this angle is multiplied by the measurement length, 1 mm, resulting in a standard uncertainty of 10 pm.

The last significant component is the uncertainty in the determination of the line position from the image data. One of the limiting factors here is the imperfection of the grating lines. In order to average over a larger section of the line image, we first superimpose and average many line images together to create an average line image. We then define the position of any individual line to be the position of maximum cross-correlation between it and the average line image. The repeatability of this method can be verified by examining different sections of the individual lines. The other limiting factor, to some extent, is the image pixel spacing. For this measurement, the X-axis pixel spacing was 5 nm. Overall, we estimate the uncertainty from this source to be 3 nm at each end of the point-to-point measurement, uncorrelated, or 5 nm combined.

These uncertainty components are summarized in Table 1. All of the uncertainty components in this budget are based on a Type B evaluation of standard uncertainty, *i.e.*, scientific judgement as opposed to statistical analysis. The individual components are combined by the root-sum-of-squares method resulting in an overall combined standard uncertainty, u_c, of 26 nm.

Table 1: M^3 Uncertainty Estimate for 1 mm Measurement

Uncertainty component	Estimated Value, EV (nm)	Comments
Wavelength of Light	0.1	$\delta\lambda/\lambda = 10^7$; EV = $(\delta\lambda/\lambda) \times 1$ mm; (believed very conservative)
Polarization Mixing	1	$\delta x = 0.5$ nm (peak); EV = $2\,\delta x$
Interferometer Cosine Error	20	Optical Path = 300 mm; Maximum beam separation at optics = 2 mm; $\theta = 2/300$; EV = $\theta^2/2 \times 1$ mm
Abbé Offset Error	9	Abbé Offset = 10 mm; $\theta = 5 \times 10^{-7}$ ea. for the X coarse, X fine, and Y fine carriages; EV = $1.73 \times \theta \times 10$ mm
Z-to-X Coupling Uncertainty	13	$\delta_{xz} = 0.10 \pm 0.02$; $Z = 650$ nm for the 1 mm displacement; EV = $Z \times \delta_{xz}$
Temperature Instability Uncertainty	4	$T = 5$ m°C; 25 mm of Cu, $CTE_{Cu} = 2 \times 10^{-5}$/°C; 25 mm of stainless steel, $CTE_{SS} = 1 \times 10^{-5}$/°C; EV = $T \times 25$ mm $\times (CTE_{Cu} + CTE_{SS})$
Specimen Cosine Error	0.01	$\theta = 10^{-4}$; EV = $\theta^2/2 \times 1$ mm
Line Center Determination	4	$\delta x = 3$ nm; EV = $1.4\,\delta x$
$\sigma = (\sum EV_i^2)^{1/2}$	26	

DESIGN MODIFICATIONS

An examination of the sources of uncertainty in the measurements suggests some areas where the machine design could be improved. Additionally, there are some elements that need to be modified to improve reliability, convenience and flexibility. We are now in the process of making these design changes.

Aside from the interferometer cosine error, which can be greatly improved without any modifications of the instrument, the largest contributor to the measurement uncertainty is the Z-to-X (and Z-to-Y) motion coupling. To address this problem, the Z-axis fine-motion scanner has been redesigned to include a flexure-constrained motion guide. This should greatly improve the linearity and the repeatability of motion. The new design also includes a capacitance gage sensor for measuring the position of the Z fine-motion stage. This allows some level of metrology in the Z-axis, and gives a reference position for mapping the Z actuator off-axis motion. The Z coarse motor had to be redesigned to accommodate the changes in the fine-motion actuator. A coarse-motion position sensor is also integrated into the new design. This will increase the convenience of operation since second approaches of the SPM tip to the same point on the specimen will be able to rely on this information instead of visual operator feedback from the internal charge-coupled device (CCD) camera. Leaving the CCD camera off also improves the thermal stability.

The next largest item in the uncertainty estimate is the Abbé offset error. The underlying problem is again one of precision motion generation. To improve the coarse-motion slideway

precision, the backup machine core is being replaced with the new core that has diamond-turned ways. A zero-position sensor is being added to provide a fixed datum for resetting the interferometers. This enables mapping the coarse-motion errors relative to the position of the carriages on the slideways. The fine-motion stages are being improved by weakening the motion-guiding flexures, thus shifting the design compromise from stiffness towards motion precision. Additionally, capacitance-gage sensors are being added for measuring the position of the fine-motion stages relative to the coarse-motion stages. This provides a reference position against which to map the motion errors of the fine-motion carriages. With these changes, error maps of the roll and pitch can be made as a function of position for both the fine- and coarse-motion carriages thus enabling measurement corrections for these effects. The uncertainty in the error maps will remain a component in the overall uncertainty.

The next biggest uncertainty component is due to temperature instability. To improve this factor, one approach is to decrease the sensitivity of the instrument to thermal changes. We are doing this by changing the material of the mounting plate from stainless steel to Invar. A platinum resistance thermometer is also being added to the mounting plate so that temperature changes in that component can be more accurately known. In the future, we may also change the material of the sample holder from copper to Invar. The other approach is to limit thermal fluctuations by eliminating large variable heat sources. The biggest heat sources in the core are the CCD camera and its illumination source and the X and Y coarse-motion motors. The CCD camera is easily accommodated by not using it during a measurement. For the X and Y coarse motion motors,

the interim rotary electromagnetic stepper motors are being replaced by linear piezoelectric motors that generate much less heat. This was not done originally because no piezoelectric motors were found that could generate enough force. We now have a custom combination of two piezoelectric motors in parallel to overcome this problem. There were also reliability problems with the interim motors that the new motors should overcome.

The remaining significant components in the uncertainty budget are the line center determination and the polarization mixing errors. To a certain extent, the precision of line center determination is a function of the perfection of the specimen, the uniformity and sharpness of the features and the straightness of the edges. Increasing the density of data points in the measurement can also be a factor in some cases, and is easily done. The polarization mixing error is fairly small. It can be dealt with by averaging over multiple measurements, with the sample repositioned within the metrology box. Alternatively, since we are operating in vacuum, it is conceivable that the polarization-mixing component will have long-term repeatability as a function of the interferometer reading, and will therefore be mappable.

We are also taking advantage of this time of rebuilding to simultaneously replace the control, data acquisition and display system. The new architecture uses multiple digital signal processors (DSPs) for controlling the various subsystems, all on a common VME backplane, as shown in Figure 4. Top-level control and data acquisition and display are done on a UNIX workstation that is connected to the VME backplane through a bus adapter. The DSPs each have separate mezzanine I/O busses and daughter cards for direct interface with the M^3 hardware, thereby avoiding potential bottlenecks on the VME bus. The DSPs also have direct serial communication ports that can be used for dedicated, off-bus, inter-processor communication. Two of the DSPs are assigned to calculating the position for the X and Y interferometers. One DSP is dedicated to X- and Y-axes scan generation and control. And the remaining DSP handles the Z axis positioners including the SPM servo control. The software for the new system takes a similar approach as for the old system. The operator interface is built into the PV-wave [12] software environment using PV-wave's command line interpreter and graphics routines. Low-level control and interface with the DSPs is through callable routines written in C.

CONCLUSIONS

We designed and built a measuring instrument with performance goals that push the state-of-the-art. Integrated functioning of all the subsystems has been demonstrated and example measurements have been performed on select artifacts. The 50 mm by 50 mm scan range goal has been achieved. Temperature control of 5 mK stability has been demonstrated during measurement scans. Sub-nanometer interferometer resolution has been achieved. Nanometer-level specimen feature resolution has been demonstrated. For a 1 mm distance measurement, an analysis of the sources of measurement uncertainty has been done, indicating an expanded uncertainty of 50 nm (k = 2). Machine modifications to lower the measurement uncertainty are now underway.
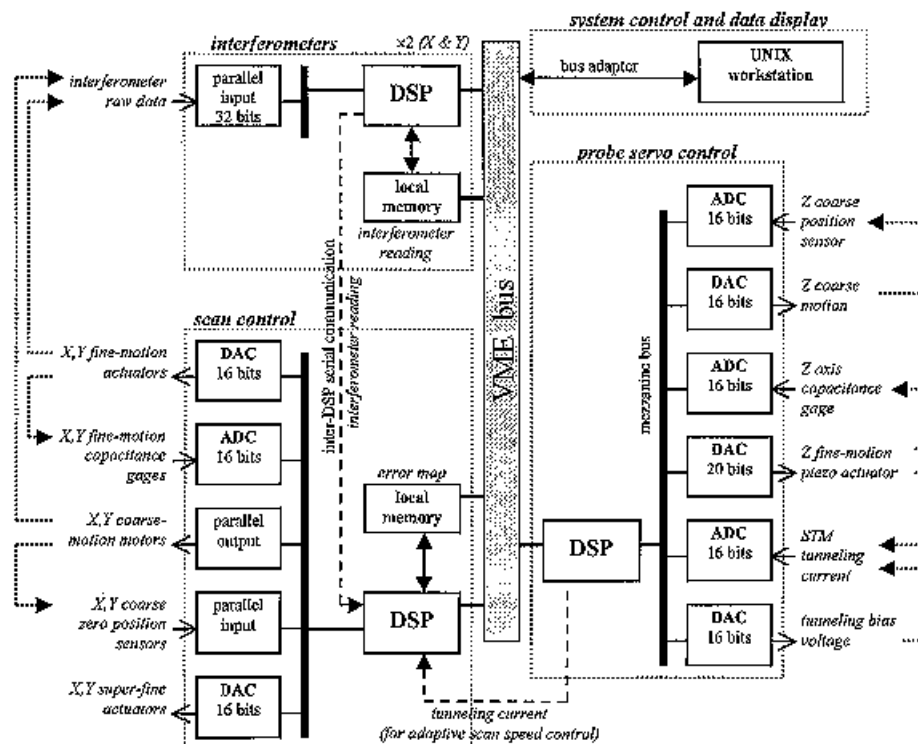

Figure 4. Block diagram of the Molecular Measuring Machine controller system.

The Molecular Measuring Machine is to be used mostly for calibration of specimens and as a tool in the development and certification of standard artifacts for use in the microelectronics, data-storage, and other high technology industries. Calibration of conventional two-dimensional grid artifacts, and two-dimensional holographic-grating artifacts is planned. We also are developing atom-based artifacts for step-height, linewidth, and pitch where the basic dimension is based on an intrinsic property of the material such as an integral number of atomic planes [13]. During development, the dimensions of some of these artifacts will be validated with M^3. Conversely, we plan to validate the geometric perfection and both the long-distance and periodic scale accuracy of the M^3 metrology system by comparing with the atomic or molecular periodicity in suitable crystals. The high-precision, high-accuracy positioning capability of M^3 may also find important applications in researching new methods of nanofabrication, where structures may be built-up or eroded one atom or molecule at a time.

ACKNOWLEDGEMENTS

REFERENCES

[1] "The National Technology Roadmap for Semiconductors, Technology Needs, 1997 Edition," Semiconductor Industry Association, 1997.

[2] E. Clayton Teague, "The National Institute of Standards and Technology molecular measuring machine project: Metrology and precision engineering design," *J. Vac. Sci. Technol. B,* Vol.7, No.6, pp. 1898-1902, 1989.

[3] Teflon is a registered trademark of DuPont. Certain commercial equipment, instruments, or materials are identified in this paper in order to specify the experimental procedure adequately. Such identification does not imply recommendation or endorsement by the National Institute of Standards and Technology, nor does it imply that the materials or equipment specified are necessarily the best available for the purpose.

[4] G. Binnig and D.P.E. Smith, "Single-tube three-dimensional scanner for scanning tunneling microscopy," *Rev. Sci. Instrum.* Vol.57, No.8, pp. 1688-1689, 1986.

[5] G.J. Siddall and R.R. Baldwin, "Developments in Laser Interferometry for Position Sensing," *Precis. Eng.*, Vol.6, pp.175-180, 1984.

[6] Laboratory for Science, model 220.

[7] Hewlett-Packard, model 5572A.

[8] N.M. Oldham, J.A. Kramar, P.S. Hetrick, and E.C. Teague, "Electronic Limitations in Phase Meters for Heterodyne Interferometry," *Precis. Eng*, Vol.15, No.3, pp. 173-179, 1993.

[9] Concurrent Computer Corporation, 6000 Series.

[10] J.J. McClelland, R.E. Scholten, E.C. Palm, and R.J. Celotta, "Laser Focused Atomic Deposition," *Science*, Vol.262, pp. 877-880, 1993.

[11] B.N. Taylor and C.E. Kuyatt, "Guidelines for Evaluating and Expressing the Uncertainty of NIST Measurement Results," NIST Technical Note 1297, 1994.

[12] Visual Numerics, Inc.

[13] V.W. Tsai, T.V. Vorburger, P. Sullivan, R. Dixson, R. Silver, E.D. Williams, and J. Schneir, "Height Calibration of Atomic Force Microscopes using Silicon Atomic Step Artifacts," *Proc. of the 11th Ann. Mtg. of the American Soc. for Precision Engineering, Raleigh, NC*, Vol. 14, pp. 212-216, 1996; Vincent Tsai, X.-S. Wang, and Ellen D. Williams, "Conformal Oxides On Si Surfaces," *Appl. Phys. Lett.*, Vol. 71, No. 11, pp. 1495-1497, 1997.